

Quantum Effects in 3+1 Schwarzschild-de Sitter Spacetime: Properties of the Hadamard Function

Ian M. Newsome,^{1,*} Silvia Pla,^{2,†} and Paul R. Anderson^{1,‡}

¹*Department of Physics, Wake Forest University, Winston-Salem, NC, 27109, USA*

²*Theoretical Particle Physics and Cosmology,*

King's College, London, WC2R 2LS, UK

(Dated: August 1, 2024)

In a four-dimensional Schwarzschild-de Sitter background, the spherically symmetric ($\ell = 0$) contribution to the Hadamard two-point correlation function is computed for a massless minimally-coupled scalar field in the Unruh state. Consideration is given to spacetime points located exterior to the black hole horizon, but within the cosmological horizon. Previously it was found in two dimensions for spatially separated points that the Hadamard function exhibits unbounded linear growth at late times, with a rate of growth proportional to the sum of the black hole and cosmological surface gravities. Here it is shown numerically that this behavior persists in four dimensions, where scattering effects associated with the scalar field modes lead to a modification of the two-dimensional result. An analytic approximation is derived for the growth rate in four dimensions and, in the limit that the black hole vanishes, the leading order contribution is equivalent to the rate of growth for the Hadamard function found previously for de Sitter space in cosmological coordinates.

* newsim18@wfu.edu

† silvia.pla_garcia@kcl.ac.uk

‡ anderson@wfu.edu

I. INTRODUCTION

Schwarzschild-de Sitter (SdS) spacetime is an exact solution to the vacuum Einstein equations in the presence of a positive cosmological constant. It describes an eternal black hole immersed in an expanding universe and contains both a black hole and cosmological horizon. As for Schwarzschild spacetime, the solution can be used to describe the late-time geometry of a black hole that forms from collapse in an exponentially expanding universe. For SdS, one expects Hawking radiation [1] related to both the black hole and cosmological horizons [2].

The Unruh state [3] is the natural state for a quantum field in an eternal black hole spacetime to describe the effects of black hole evaporation associated with a black hole which forms from collapse. Its generalization to SdS has been given in [4, 5]. In particular, for SdS one can associate with each horizon radiation which exhibits a thermal distribution with temperature $T = \kappa/2\pi$, where κ is the magnitude of the black hole or cosmological horizon surface gravity, which in general are not equal.

It is interesting to study the behaviors of the quantum field modes which comprise the Unruh state. For a massless minimally-coupled scalar field in two dimensions (2D), there is no scattering and it is trivial to show that, in the usual static coordinates, the mode functions for the Unruh state approach constant values at late times for fixed values of the spatial coordinate. In contrast, for a massive minimally-coupled scalar field in 2D SdS it was found [6] that the corresponding mode functions for the Unruh state vanish at late times for fixed values of the spatial coordinate. This was also found generically for 2D Schwarzschild spacetime when a delta function effective potential is present in the mode equation. In both cases one can write the modes for the Unruh state in terms of packets of modes for the Boulware state (see e.g. [6]). The difference between the late time behaviors of the Unruh state modes was shown to be correlated with the fact that, for a massless minimally-coupled scalar field in 2D, there are no scattering effects and therefore the infrared divergence present in the Boulware state modes, originating from normalization, persists. In contrast, for the case of a massive minimally-coupled scalar field in 2D SdS or a massless minimally-coupled scalar field in 2D Schwarzschild with a delta function potential, scattering effects remove the infrared divergences in the Boulware modes.

The behavior of the symmetric two-point function, or Hadamard function, has been inves-

tigated in 2D for SdS and other spacetimes containing black hole or cosmological horizons [7]. It was found that the existence of a past black hole and/or past cosmological horizon results in late-time unbounded linear growth of the Hadamard function in a region described by a static metric for points that are spatially separated along a constant time hypersurface in the coordinate system which gives that metric. The Hadamard function rate of growth for 2D SdS was found to be

$$R_{2D} \equiv \frac{d}{dt} G^{(1)}(t, r; t, r') = \frac{1}{2\pi} (\kappa_b + \kappa_c) \quad , \quad (1.1)$$

where κ_b and κ_c are the surface gravities associated with the black hole and cosmological horizons, respectively. It was found that no such growth in time occurs in 2D Schwarzschild if there is scattering due to a delta function effective potential present in the mode equation [6].

In this paper, the question of whether the above effects found in 2D SdS for a massless minimally-coupled scalar field persist in four dimensions (4D) is addressed. Consideration is given to the spherically symmetric ($\ell = 0$) modes which contribute to the Unruh state. These modes are of particular interest because previous work has shown that scattering effects do not cause the grey-body factors for these modes to vanish in the zero frequency limit [9, 10], nor do they remove the infrared divergences in the Boulware modes [11]. In contrast, for $\ell > 0$ the gray-body factors vanish in the zero frequency limit [12, 13] and therefore it is extremely likely that the infrared divergences in the Boulware modes will also be removed. In parallel with the previous 2D SdS calculation, spacetime points located between the black hole and cosmological horizons will be considered.

This paper is organized as follows. In Sec. II, a review of SdS spacetime is given with a formulation of the quantum states and mode equation required for computation of the Hadamard function. In Sec. III and IV, numerical results for the 4D Kruskal modes and the Hadamard function, respectively, are presented. An analytic approximation for the growth rate associated with the 4D Hadamard function is derived in Sec. V, including its predictions and comparisons between the 4D numerical and 2D analytic results. A summary and discussion of the results is given in Sec. VI.

II. QUANTUM STATES AND MODE DECOMPOSITION IN 3+1 SCHWARZSCHILD-DE SITTER

The metric for a 4D SdS spacetime in terms of the usual static coordinates is

$$ds^2 = -f(r)dt^2 + \frac{1}{f(r)}dr^2 + r^2 (d\theta^2 + \sin^2\theta d\phi^2) \quad , \quad (2.1)$$

with

$$f(r) = 1 - \frac{2M}{r} - H^2 r^2 = -\frac{H^2}{r}(r - r_b)(r - r_c)(r + r_b + r_c) \quad . \quad (2.2)$$

Here M is the black hole mass, $H^2 = \Lambda/3$ with Λ the positive cosmological constant, and the black hole and cosmological horizon radii are r_b and r_c respectively. Here and throughout, the unit convention $\hbar = c = G = 1$ is used. A Penrose diagram for the SdS spacetime is given in Fig. 1. From the relation (2.2), one finds

$$r_c = -\frac{r_b}{2} + \frac{1}{H}\sqrt{1 - \frac{3H^2 r_b^2}{4}} \quad . \quad (2.3)$$

Note that $r_c = 1/H$ if $r_b = 0$, and that r_c decreases as r_b increases. The black hole and cosmological horizons merge when $r_b = 1/\sqrt{3}H$.

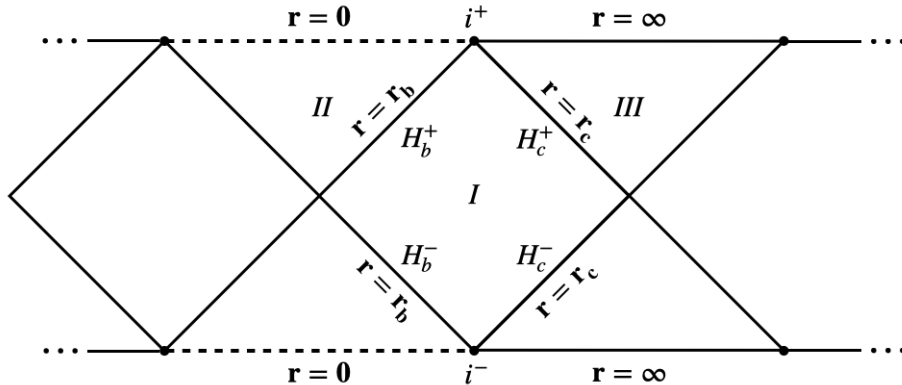


Figure 1. Penrose diagram depicting Schwarzschild-de Sitter spacetime. The past black hole and cosmological horizons are denoted $H_{(b,c)}^-$ while the future horizons are denoted $H_{(b,c)}^+$. The static patch is indicated by region I , whereas the black hole interior and cosmological far-field region are indicated by II and III respectively.

The general form of the Hadamard function in terms of a massless minimally-coupled scalar field ϕ at distinct spacetime points x, x' is given by

$$G^{(1)}(x, x') = \langle \{ \phi(x), \phi(x') \} \rangle \quad , \quad (2.4)$$

where the scalar field ϕ satisfies

$$\square\phi(x) = \frac{1}{\sqrt{-g}}\partial_\mu\left[\sqrt{-g}\partial^\mu\phi(x)\right] = 0 \quad . \quad (2.5)$$

Calculation of $G^{(1)}(x, x')$ in the static patch (region I of Fig. 1) requires the expansion of the scalar field ϕ in terms of a complete set of modes associated with a particular quantum state. The modes associated with the generalized SdS Unruh vacuum are defined on the Cauchy surface consisting of $H_b^- \cup H_c^-$, with $H_{(b,c)}^-$ the past black hole and cosmological horizons. On this Cauchy surface, the modes $p_{\omega\ell m}^b$ and $p_{\omega\ell m}^c$ that comprise this basis are

$$p_{\omega\ell m}^b(x) = \frac{1}{\sqrt{4\pi\omega}} \frac{e^{-i\omega U_b}}{r_b} Y_{\ell m}(\theta, \phi) \quad \text{on } H_b^- \quad , \quad (2.6a)$$

$$p_{\omega\ell m}^c(x) = \frac{1}{\sqrt{4\pi\omega}} \frac{e^{-i\omega V_c}}{r_c} Y_{\ell m}(\theta, \phi) \quad \text{on } H_c^- \quad , \quad (2.6b)$$

where U_b and V_c are the Kruskal coordinates associated with H_b^- and H_c^- , respectively. Note that hereafter $p_{\omega\ell m}^{(b,c)}$ are referred to as Kruskal modes. The scalar field representation for the Unruh state is

$$\phi(x) = \sum_{\ell=0}^{\infty} \sum_{m=-\ell}^{\ell} \int_0^{\infty} d\omega \left[a_{\omega\ell m}^b p_{\omega\ell m}^b(x) + a_{\omega\ell m}^{b\dagger} p_{\omega\ell m}^{b*}(x) + a_{\omega\ell m}^c p_{\omega\ell m}^c(x) + a_{\omega\ell m}^{c\dagger} p_{\omega\ell m}^{c*}(x) \right] \quad , \quad (2.7)$$

where $[a_{\omega\ell m}^h, a_{\omega'\ell'm'}^{h\dagger}] = \delta(\omega - \omega') \delta_{\ell,\ell'} \delta_{m,m'} \delta_{h,h'}$ with $h = b, c$. It follows that the Hadamard function (2.4) for the Unruh state is

$$G^{(1)}(x, x') = 2 \sum_{\ell=0}^{\infty} \sum_{m=-\ell}^{\ell} \int_0^{\infty} d\omega \operatorname{Re} \left\{ p_{\omega\ell m}^b(x) p_{\omega\ell m}^{b*}(x') + p_{\omega\ell m}^c(x) p_{\omega\ell m}^{c*}(x') \right\} \quad . \quad (2.8)$$

The wave equation (2.5) is not separable in either set of Kruskal coordinates. However, in terms of the static coordinates in (2.1), it is separable and a complete set of solutions can be obtained in terms of the modes which comprise the Boulware¹ state. These modes are defined by their behaviors on the past horizons

$$h_{\omega\ell m}^b(x) = \frac{1}{\sqrt{4\pi\omega}} \frac{e^{-i\omega u}}{r_b} Y_{\ell m}(\theta, \phi) \quad \text{on } H_b^- \quad , \quad (2.9a)$$

$$h_{\omega\ell m}^c(x) = \frac{1}{\sqrt{4\pi\omega}} \frac{e^{-i\omega v}}{r_c} Y_{\ell m}(\theta, \phi) \quad \text{on } H_c^- \quad . \quad (2.9b)$$

¹ Here the natural generalization of the Boulware state from that in Schwarzschild spacetime [14] is used.

The Kruskal coordinates U_b and V_c used to define the Unruh state are related to the null coordinates $u = t - r_*$ and $v = t + r_*$, with $dr_* = dr/f$, through the relations

$$U_b(t, r) = -\frac{1}{\kappa_b} e^{-\kappa_b u(t, r)} \quad , \quad r > r_b \quad , \quad (2.10a)$$

$$V_c(t, r) = -\frac{1}{\kappa_c} e^{-\kappa_c v(t, r)} \quad , \quad r < r_c \quad . \quad (2.10b)$$

As in [7], the surface gravity associated with a particular horizon $r = r_h$ is defined to be $2\kappa_h = |f'(r_h)|$ so that all surface gravities denote positive quantities. One finds that

$$\kappa_b = \frac{H^2}{2r_b} (r_c - r_b)(2r_b + r_c) \quad , \quad (2.11a)$$

$$\kappa_c = \frac{H^2}{2r_c} (r_c - r_b)(r_b + 2r_c) \quad , \quad (2.11b)$$

$$\kappa_N = \frac{H^2}{2(r_b + r_c)} (r_b + 2r_c)(2r_b + r_c) \quad . \quad (2.11c)$$

The quantity κ_N denotes the surface gravity associated with the negative root of (2.2), namely $r_N = -(r_b + r_c)$. An explicit form for r_* is [7]

$$\begin{aligned} r_*(r) = & \frac{1}{2\kappa_b} \ln \left\{ \frac{|r - r_b|}{r_c - r_b} \right\} - \frac{1}{2\kappa_c} \ln \left\{ \frac{|r - r_c|}{r_c - r_b} \right\} + \frac{1}{2\kappa_N} \ln \left\{ \frac{r + r_c + r_b}{r_c + 2r_b} \right\} \\ & - \frac{r_c}{4r_b\kappa_b} \ln \left\{ \frac{2r_c + r_b}{r_c + 2r_b} \right\} - \frac{r_b r_c}{2(r_c - r_b)} \ln \left\{ \frac{r_b}{r_c} \right\} \quad . \end{aligned} \quad (2.12)$$

The expansions of the Kruskal modes $p_{\omega\ell m}^{(b,c)}$ in terms of the Boulware modes $h_{\omega'\ell'm'}^{(b,c)}$ can be written in the form

$$p_{\omega\ell m}^{(b,c)}(x) = \sum_{\ell'=0}^{\infty} \sum_{m'=-\ell'}^{\ell'} \int_0^{\infty} d\omega' \left[\alpha_{\omega\ell m \omega'\ell'm'}^{(b,c)} h_{\omega'\ell'm'}^{(b,c)}(x) + \beta_{\omega\ell m \omega'\ell'm'}^{(b,c)} h_{\omega'\ell'm'}^{(b,c)*}(x) \right] \quad . \quad (2.13)$$

Here $\alpha^{(b,c)}$ and $\beta^{(b,c)}$ are Bogolubov coefficients, which can be computed using the scalar product whose general form is

$$(f_1, f_2) = -i \int_{\Sigma} d\Sigma^{\mu} \sqrt{-g_{\Sigma}} f_1 \overleftrightarrow{\partial}_{\mu} f_2^* \quad , \quad (2.14)$$

where $f_{1,2}$ are any two solutions to (2.5), Σ is a Cauchy surface, and $d\Sigma^{\mu} \equiv d\Sigma n^{\mu}$ with n^{μ} the unit normal vector to Σ . Further details can be found in [15], where it is shown that the Bogolubov coefficients are partially diagonal in the sense that $\alpha_{\omega\ell m \omega'\ell'm'} \sim \delta_{\ell,\ell'} \delta_{m,m'}$ and

$\beta_{\omega\ell m\omega'\ell'm'} \sim (-1)^m \delta_{\ell,\ell'} \delta_{m,-m'}$. The results are easily adapted to the case herein allowing for a simplification of (2.13) to the following

$$p_{\omega\ell m}^{(b,c)}(x) = \int_0^\infty d\omega' \left[\alpha_{\omega\omega'}^{(b,c)} h_{\omega'\ell m}^{(b,c)}(x) + \beta_{\omega\omega'}^{(b,c)} h_{\omega'\ell(-m)}^{(b,c)*}(x) \right] . \quad (2.15)$$

Using (2.14) and the orthonormality of the modes $h_{\omega'\ell m}^{(b,c)}$ with respect to the scalar product, the explicit forms of $\alpha_{\omega\omega'}^{(b,c)}$ and $\beta_{\omega\omega'}^{(b,c)}$ are found to be [6]

$$\alpha_{\omega\omega'}^{(b,c)} = \frac{\sqrt{\omega'}}{2\pi\sqrt{\omega}} \left(\frac{1}{\kappa_{(b,c)}} \right)^{1+i\omega'/\kappa_{(b,c)}} (\epsilon - i\omega)^{i\omega'/\kappa_{(b,c)}} \Gamma \left(\delta - \frac{i\omega'}{\kappa_{(b,c)}} \right) , \quad (2.16a)$$

$$\beta_{\omega\omega'}^{(b,c)} = \frac{\sqrt{\omega'}}{2\pi\sqrt{\omega}} \left(\frac{1}{\kappa_{(b,c)}} \right)^{1-i\omega'/\kappa_{(b,c)}} (\epsilon - i\omega)^{-i\omega'/\kappa_{(b,c)}} \Gamma \left(\delta + \frac{i\omega'}{\kappa_{(b,c)}} \right) , \quad (2.16b)$$

where ϵ and δ are integrating factors such that $0 < (\epsilon, \delta) \ll 1$. For points in the static patch, the Boulware modes have the general form

$$h_{\omega'\ell m}^{(b,c)}(x) = \frac{1}{\sqrt{4\pi\omega'}} \frac{\psi_{\omega'\ell}^{(b,c)}(t, r)}{r} Y_{\ell m}(\theta, \varphi) , \quad (2.17)$$

with

$$\psi_{\omega'\ell}^{(b,c)}(t, r) = e^{-i\omega't} \chi_{\omega'\ell}^{(b,c)}(r) . \quad (2.18)$$

The radial mode functions are solutions to the equation

$$\frac{d^2}{dr_*^2} \chi_{\omega'\ell}^{(b,c)}(r) + \left[\omega'^2 - V_{\text{eff}}(r) \right] \chi_{\omega'\ell}^{(b,c)}(r) = 0 , \quad (2.19)$$

with the effective potential

$$V_{\text{eff}}(r) = f(r) \left[\frac{1}{r} \frac{d}{dr} f(r) + \frac{\ell(\ell+1)}{r^2} \right] . \quad (2.20)$$

Note that $V_{\text{eff}} \rightarrow 0$ on the black hole and cosmological horizons.² The effective potential for the spherically symmetric case, $\ell = 0$, is plotted in Fig. 2.

In order to numerically solve (2.19), two linearly independent solutions $\chi_{(R,L)}^\infty$ can be constructed which, for $r \rightarrow r_c$, have the following asymptotic behaviors

$$\chi_R^\infty(r) = e^{i\omega'r_*} , \quad (2.21a)$$

$$\chi_L^\infty(r) = e^{-i\omega'r_*} . \quad (2.21b)$$

² Since $H_b^- \cup H_c^-$ can be taken as a Cauchy surface with $V_{\text{eff}} = 0$ on both past horizons, the general forms of the Bogolubov coefficients in terms of κ are the same for any static black hole spacetime in 2D or 4D, to within an unimportant phase.

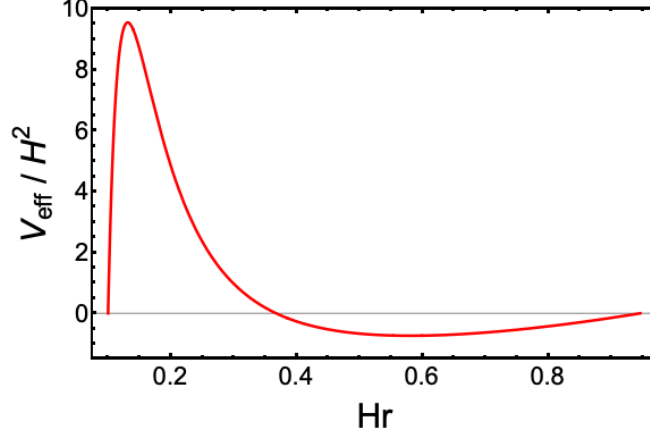


Figure 2. The effective potential V_{eff}/H^2 for $\ell = 0$, between the black hole and cosmological horizons $Hr_b = 0.1$ and $Hr_c \approx 0.95$, respectively.

Since $V_{\text{eff}} = 0$ on H_b^- , approaching the black hole horizon $r = r_b$ the solutions take the general form

$$\chi_R^\infty(r) = E_R(\omega')e^{i\omega'r_*} + F_R(\omega')e^{-i\omega'r_*} \quad , \quad (2.22a)$$

$$\chi_L^\infty(r) = E_L(\omega')e^{i\omega'r_*} + F_L(\omega')e^{-i\omega'r_*} \quad , \quad (2.22b)$$

where $E_{(R,L)}$ and $F_{(R,L)}$ are scattering parameters that can be determined numerically. The Wronskian between χ_R^∞ and χ_L^∞ can be used to show that they satisfy the relation $E_R F_L - E_L F_R = 1$. The combinations of $\chi_{(R,L)}^\infty$ which yield the radial contribution to the Boulware modes $\chi_{\omega'\ell}^{(b,c)}$ are [6]

$$\chi_{\omega'\ell}^b(r) = \frac{\chi_R^\infty(r)}{E_R(\omega')} \quad , \quad (2.23a)$$

$$\chi_{\omega'\ell}^c(r) = \chi_L^\infty(r) - \frac{E_L(\omega')}{E_R(\omega')} \chi_R^\infty(r) \quad . \quad (2.23b)$$

The Boulware modes (2.17) can therefore be expressed as

$$h_{\omega'\ell m}^b(x) = \frac{e^{-i\omega't}}{r\sqrt{4\pi\omega'}} \frac{\chi_R^\infty(r)}{E_R(\omega')} Y_{\ell m}(\theta, \phi) \quad , \quad (2.24a)$$

$$h_{\omega'\ell m}^c(x) = \frac{e^{-i\omega't}}{r\sqrt{4\pi\omega'}} \left[\chi_L^\infty(r) - \frac{E_L(\omega')}{E_R(\omega')} \chi_R^\infty(r) \right] Y_{\ell m}(\theta, \phi) \quad . \quad (2.24b)$$

III. KRUSKAL MODE SOLUTIONS

In this section, certain results of numerical computations of the Kruskal modes (2.15) for $\ell = 0$ are presented and analyzed. The numerical computations have been done for the choice of horizon radii $Hr_b = 0.1$ and $Hr_c \approx 0.95$.

In order to minimize phase effects, the magnitudes of the black hole and cosmological modes $|p_{\omega 00}^b|$ and $|p_{\omega 00}^c|$ are shown in Fig. 3 as a function of the frequency ω for the time $Ht = 0$ and the radial location $Hr = 0.3$. Note that for this location $V_{\text{eff}} > 0$. For comparison, the case when there is no scattering is also shown in which V_{eff} is artificially set equal to zero. It follows that the Kruskal mode solutions at the past horizons (2.6) are the solutions for all spacetime points and $|p_{\omega 00}^b| = |p_{\omega 00}^c| = Y_{00}/r\sqrt{4\pi\omega}$. It is clear that scattering

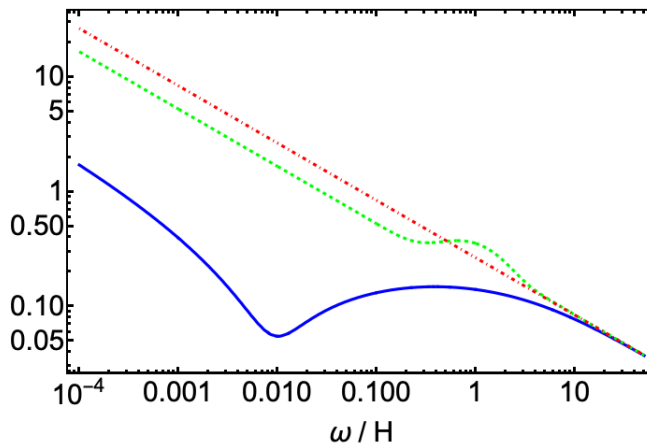


Figure 3. The magnitudes $|H^{-1/2} p_{\omega 00}^b|$ (blue-solid) and $|H^{-1/2} p_{\omega 00}^c|$ (green-dashed), as well as the case for which scattering effects have been ignored (red-dot-dashed), are shown as a function of the frequency ω/H . All mode data is evaluated at time $Ht = 0$ for a radial location $Hr = 0.3$ between the horizons $Hr_b = 0.1$ and $Hr_c \approx 0.95$.

effects result in a suppression of the modes at sufficiently small frequencies compared with their values when scattering effects are absent. Furthermore, there is a significant suppression of the black hole mode amplitudes for $\omega/H \lesssim 1$ as compared to the cosmological modes, with a local minimum in the black hole mode amplitude occurring for $\omega/H \approx 10^{-2}$. However, the infrared divergence originating from normalization can be observed for both $p_{\omega 00}^b$ and $p_{\omega 00}^c$. For frequencies $\omega/H \sim 1$, an amplification of the cosmological mode amplitudes compared to that of the no-scattering case can also be observed. The high frequency behavior $\omega/H \gg 1$

is such that both the black hole and cosmological modes approach their no-scattering form (2.6).

As can be seen in Fig. 2, V_{eff} is largest relatively close to the black hole horizon. Therefore, the propagation of the Boulware modes $h_{\omega'\ell m}^b$ from the past black hole horizon into the static patch will be influenced more significantly by scattering effects than the modes $h_{\omega'\ell m}^c$ propagating from the past cosmological horizon. Since $p_{\omega\ell m}^{(b,c)}$ in (2.15) can be written in terms of packets of the modes $h_{\omega'\ell m}^{(b,c)}$, a deficiency in the black hole Boulware mode $h_{\omega'\ell m}^b$ contribution will be expressed as a smaller amplitude for the oscillations of $p_{\omega\ell m}^b$ for a given frequency $\omega'^2 \lesssim V_{\text{eff}}$.

A significant factor related to the difference in properties between the $p_{\omega 00}^b$ and $p_{\omega 00}^c$ modes originates from the radius of the black hole horizon relative to the cosmological horizon. The relative horizon sizes dictate the magnitude of the effective potential responsible for scattering effects of the Boulware modes and furthermore, for the spherically symmetric case, the effective potential can be either positive or negative depending upon the radial coordinate chosen. Note, for $\ell > 0$ the effective potential (2.20) is strictly positive. A more comprehensive analysis concerning the effect of scattering on the Boulware modes due to the presence of an effective potential, and by extension its connection with the Kruskal modes is the subject of future investigation.

The time evolution of the modes $p_{\omega 00}^b$ and $p_{\omega 00}^c$ is represented in both Fig. 4 and Fig. 5. The former shows the real and imaginary components of the black hole mode $p_{\omega 00}^b$ for a single frequency $\omega/H = 10^{-1}$, while the latter shows the magnitude of the real parts of $p_{\omega 00}^b$ and $p_{\omega 00}^c$ for a variety of frequencies ω . All modes are evaluated at the radial coordinate $Hr = 0.5$. Note that for this location $V_{\text{eff}} < 0$.

From Fig. 4, it can be seen that both the real and imaginary parts of $p_{\omega 00}^b$ exhibit early-time oscillatory behavior which at later times transitions to a constant value. The late-time constant value associated with the real part of $p_{\omega 00}^b$ is nonzero, while that of the imaginary part is zero. The timescale for which each reaches their respective late-times values is the same. Although not shown, the imaginary parts of both the black hole and cosmological Kruskal modes for any frequency ω will tend to zero over a timescale which coincides with the real part of a given mode going to its late-time nonzero constant value.

In Fig. 5 it can be seen, for all frequencies considered, that at sufficiently late times the real parts of $p_{\omega 00}^b$ and $p_{\omega 00}^c$ approach nonzero constant values, which decrease exponentially

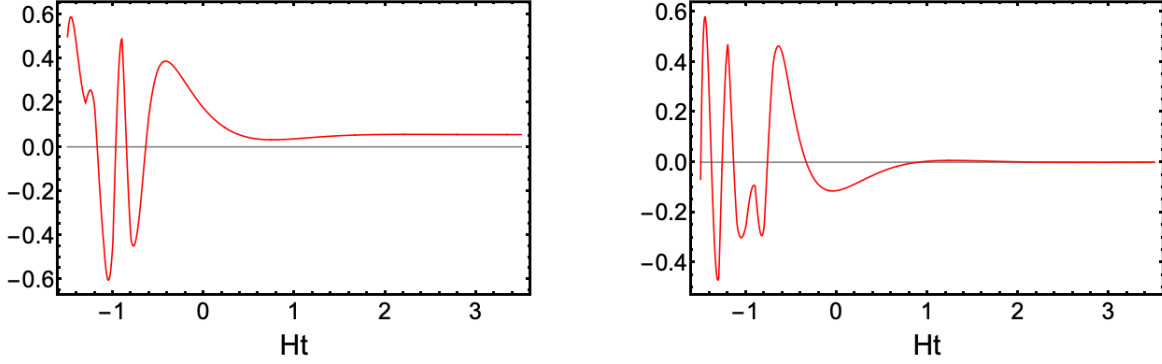


Figure 4. The late time behavior is shown for the real (left) and imaginary (right) parts of the black hole Kruskal mode $H^{-1/2} p_{\omega 00}^b$ for frequency $\omega/H = 10^{-1}$. Both plots are evaluated at a radial coordinate value $Hr = 0.5$ between the horizons $Hr_b = 0.1$ and $Hr_c \approx 0.95$.

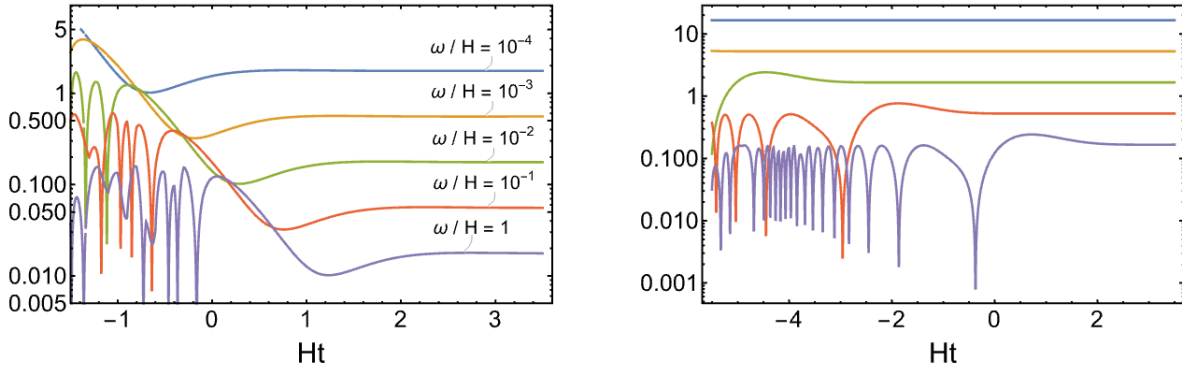


Figure 5. The late time behavior is shown for the magnitude of the real parts of the black hole Kruskal modes (left) and cosmological (right) Kruskal modes $H^{-1/2} p_{\omega 00}^{(b,c)}$, for a variety of frequencies in the range $10^{-4} \leq \omega/H \leq 1$. Both plots are evaluated at a radial coordinate value $Hr = 0.5$ between the horizons $Hr_b = 0.1$ and $Hr_c \approx 0.95$. Note that for the plot of $H^{-1/2} p_{\omega 00}^c$, the curves match the frequency order in which the plot of $H^{-1/2} p_{\omega 00}^b$ is presented.

in the frequency. However, the time required for the modes to achieve a constant value increases linearly as the frequency is increased. Another feature that emerges is a branch which partitions the early time oscillatory behavior of the $p_{\omega 00}^b$ modes from their late time approach to a constant value. As a given mode evolves through this region, there is an exponential decrease in its value and the duration in time spent on the branch appears to be constant for all frequencies considered. A careful analysis shows a similar, but less

pronounced, behavior for the real parts of the $p_{\omega 00}^c$ modes. In contrast with the $p_{\omega 00}^b$ modes, the frequency dependent, late time constant values approached by the real parts of the $p_{\omega 00}^c$ modes are consistently larger for all frequencies ω . Furthermore, there exists a larger spacing in both the constant values that the $p_{\omega 00}^c$ modes approach at late times for different frequencies ω , as well as the time required for them to approach these values, which becomes smaller as ω decreases.

IV. THE HADAMARD FUNCTION

The late-time approach to a nonzero constant value for either set of modes $p_{\omega 00}^b$ or $p_{\omega 00}^c$ has a significant effect on the Hadamard function. As evidenced previously for a variety of 2D spacetimes [6], infrared effects associated with the Boulware modes $h_{\omega' 00}^{(b,c)}$ have a significant impact on the late time properties of the Kruskal modes $p_{\omega 00}^{(b,c)}$, and by extension on the behavior of the Hadamard function. Namely, if scattering does not remove the infrared divergences present in the Boulware modes, then the Kruskal modes will approach nonzero constant values at late times, leading to unbounded linear growth in time for the Hadamard function. In 4D SdS with no scattering, this nonzero constant value for the Kruskal modes is $p_{\omega 00}^{(b,c)} = Y_{00}/r\sqrt{4\pi\omega}$.

The $\ell = 0$ contribution to the Hadamard function (2.8) is plotted as a function of the static time coordinate t in Fig. 6 for spacelike separated radial points $Hr = 0.3$ and $Hr' = 0.5$ between horizons $Hr_b = 0.1$ and $Hr_c \approx 0.95$. There is clear linear growth over the times considered.

To see the effect of position on the 4D Hadamard growth rate, multiple radial coordinate pairs in the static patch were investigated, including pairs of points where V_{eff} changes sign. To within two significant digits the growth rate, numerically determined to be $\frac{d}{dt} G^{(1)}(t, r, \theta, \phi; t, r', \theta', \phi') = 0.052 H^3$, is constant for all radial coordinate pairs considered, providing strong evidence that not only the linear instability persists in 4D, but the growth rate for given values of r_b and r_c is independent of the radial coordinates r, r' .

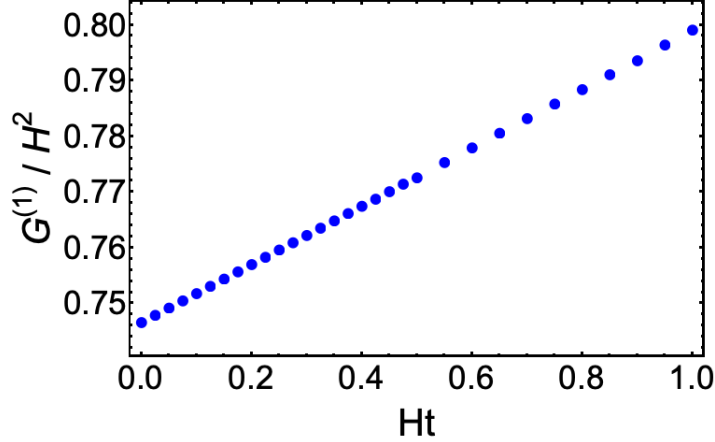


Figure 6. Numerical solutions for the $\ell = 0$ contribution to the 4D Hadamard function $G^{(1)}/H^2$ are shown as a function of Ht for a radial coordinate pair $Hr = 0.3$ and $Hr' = 0.5$ between the horizons $Hr_b = 0.1$ and $Hr_c \approx 0.95$.

V. ANALYTIC FORM OF THE 4D HADAMARD FUNCTION

Having established numerical evidence for the presence of unbounded linear growth originating from the $\ell = 0$ contribution to the 4D Hadamard function, an analytic approximation will now be derived for the growth rate. There are two key points which make it possible to find such an approximation. The first is that for large enough values of ω for any fixed spacetime point, the integral in (2.15) for a given Kruskal mode can be evaluated using the stationary phase approximation. In this case, it will be shown that the contribution of the modes to (2.8) with similar frequencies will oscillate rapidly in ω for late times and fixed values of the spatial coordinates, yielding a relatively small contribution. The dominant contribution to (2.8) at late times comes from those Kruskal modes with a relatively small frequency ω . For these modes there is no stationary phase point and the dominant contribution to (2.15) comes from the singularity in the integrand at $\omega' = 0$.

To determine the condition for a stationary phase point to exist, first note that the $\ell = 0$ contribution to the integrand in (2.15) is of the form $\alpha_{\omega\omega'}^{(b,c)} h_{\omega'00}^{(b,c)} + \beta_{\omega\omega'}^{(b,c)} h_{\omega'00}^{(b,c)*}$. Stationary phase points for the resulting frequency integrals occur if Stirling's approximation

$$\Gamma(z) \approx \sqrt{2\pi} z^{z-1/2} e^{-z} \quad , \quad (5.1)$$

is valid for the gamma functions in their integrands, which occurs if $\omega' \gg \kappa_{(b,c)}$. There will be minimum values of ω for which a stationary phase point exists for $p_{\omega 00}^b$ and $p_{\omega 00}^c$

and these will be denoted by $\omega'_{\text{S.P. min}}{}^b$ and $\omega'_{\text{S.P. min}}{}^c$, respectively. Thus, the stationary phase points found using Sterling's approximation satisfy the condition

$$\omega'_{\text{S.P.}} \geq \omega'_{\text{S.P. min}}{}^{(b,c)} \gg \kappa_{(b,c)} \quad . \quad (5.2)$$

Furthermore, if in (2.19) one considers frequencies such that $\omega'_{\text{S.P.}}{}^2 \gg |V_{\text{eff}}|_{\text{max}}$ then the radial parts of the Boulware modes will be approximately equal to their no-scattering forms, i.e.

$$\chi_{\omega'0}^{(b,c)} \approx e^{\pm i\omega' r_*} \quad . \quad (5.3)$$

For the values of ω' used for the numerical computations shown in this paper, this condition is always satisfied by the stationary phase points if Stirling's approximation is valid.

If one partitions the ω' -integral present in (2.15) into separate frequency regimes of the form

$$\int_0^\infty y d\omega' = \int_0^\lambda y d\omega' + \int_\lambda^\Lambda y d\omega' + \int_\Lambda^\infty y d\omega' \quad , \quad (5.4)$$

where Λ is large enough that the no-scattering solutions can be used for the modes, then to leading order the contributions to the Kruskal modes from the third integral are

$$p_{\omega 00}^{(b,c)}(x)_{\text{high}} \approx \frac{e^{\frac{i\pi}{4}}}{\sqrt{32\pi^3\omega r}} \int_\Lambda^\infty \frac{d\omega'}{\sqrt{\omega'}} e^{i\Phi_\alpha^{(b,c)}(\omega')} + \frac{e^{-\frac{i\pi}{4}}}{\sqrt{32\pi^3\omega r}} \int_\Lambda^\infty \frac{d\omega'}{\sqrt{\omega'}} e^{-\frac{\pi\omega'}{\kappa_{(b,c)}}} e^{i\Phi_\beta^{(b,c)}(\omega')} \quad , \quad (5.5)$$

with

$$\Phi_\alpha^b(\omega') = -\Phi_\beta^b(\omega') = \frac{\omega'}{\kappa_b} \left(\ln \left\{ \frac{\omega}{\omega'} \right\} + 1 \right) - \omega' u \quad , \quad (5.6a)$$

$$\Phi_\alpha^c(\omega') = -\Phi_\beta^c(\omega') = \frac{\omega'}{\kappa_c} \left(\ln \left\{ \frac{\omega}{\omega'} \right\} + 1 \right) - \omega' v \quad . \quad (5.6b)$$

From (5.6), one can implement the condition for stationary phase $d\Phi(\omega')/d\omega' = 0$ to find the stationary phase points

$$\omega'_{\text{S.P.}}{}^b \approx \omega e^{-\kappa_b u} \quad , \quad (5.7a)$$

$$\omega'_{\text{S.P.}}{}^c \approx \omega e^{-\kappa_c v} \quad . \quad (5.7b)$$

Substituting (5.7) into (5.2), one finds that there is a stationary phase approximation for $p_{\omega 00}^b$ and $p_{\omega 00}^c$ only if

$$\omega^b \geq e^{\kappa_b u} \omega'_{\text{S.P. min}}{}^b \quad , \quad (5.8a)$$

$$\omega^c \geq e^{\kappa_c v} \omega'_{\text{S.P. min}}{}^c \quad . \quad (5.8b)$$

As a result, the $\ell = 0$ contribution to the Hadamard function in (2.8) can be divided into four parts such that

$$\begin{aligned} \frac{1}{2}G^{(1)}(x, x') &= \int_0^{e^{\kappa_b u} \omega'_{\text{S.P. min}}{}^b} d\omega \operatorname{Re} \left\{ p_{\omega 00}^b(x) p_{\omega 00}^{b*}(x') \right\} + \int_{e^{\kappa_b u} \omega'_{\text{S.P. min}}{}^b}^{\infty} d\omega \operatorname{Re} \left\{ p_{\omega 00}^b(x) p_{\omega 00}^{b*}(x') \right\} \\ &+ \int_0^{e^{\kappa_c v} \omega'_{\text{S.P. min}}{}^c} d\omega \operatorname{Re} \left\{ p_{\omega 00}^c(x) p_{\omega 00}^{c*}(x') \right\} + \int_{e^{\kappa_c v} \omega'_{\text{S.P. min}}{}^c}^{\infty} d\omega \operatorname{Re} \left\{ p_{\omega 00}^c(x) p_{\omega 00}^{c*}(x') \right\}. \end{aligned} \quad (5.9)$$

For the second and fourth integrals in (5.9), the stationary phase approximation can be used to compute $p_{\omega 00}^b$ and $p_{\omega 00}^c$. The result is that those integrals oscillate rapidly in ω at late times and make only a small contribution to the Hadamard function. The primary contribution at late times therefore comes from the first and third integrals.

There is no stationary phase point in the integrands for $p_{\omega 00}^{(b,c)}$ in (2.15) for the values of ω in the first and third integrals. At late times the dominant contributions to the integrals originates from the range $0 \leq \omega' \leq \lambda$, for some λ which becomes smaller as u or v increases for fixed ω . The solutions $\chi_{(R,L)}^{\infty}$ to the radial mode equation (2.19) in this small frequency regime have the form [6, 11]

$$\chi_R^{\infty}(r) = \chi_L^{\infty*}(r) = \chi_0^{(1)}(r) + i\omega' \chi_0^{(2)}(r) \quad , \quad (5.10)$$

where $\chi_0^{(1)}$ and $\chi_0^{(2)}$ are solutions to (2.19) for $\omega' = 0$ of the form

$$\chi_0^{(1)}(r) = \frac{r}{r_c} \quad , \quad (5.11a)$$

$$\chi_0^{(2)}(r) = ar + r_c r \int_r \frac{dr'}{r' f(r')} \quad , \quad (5.11b)$$

with a an arbitrary constant. Furthermore, as shown in [11], one has for $\ell = 0$

$$\lim_{\omega' \rightarrow 0} E_R(\omega') = \frac{1}{2} \left(\frac{r_b^2 + r_c^2}{r_b r_c} \right) \quad , \quad (5.12a)$$

$$\lim_{\omega' \rightarrow 0} E_L(\omega') = \frac{1}{2} \left(\frac{r_b^2 - r_c^2}{r_b r_c} \right) \quad . \quad (5.12b)$$

Therefore, using the definition of the Boulware modes in (2.24), one finds for small values of ω' that

$$h_{\omega' 00}^{(b,c)}(x) \approx \frac{1}{2\pi \sqrt{\omega'}} \left(\frac{r^{(b,c)}}{r_b^2 + r_c^2} \right) e^{-i\omega' t} \quad . \quad (5.13)$$

The associated Bogolubov coefficients (2.16) present in (2.15) satisfy the relationship $\left(\beta_{\omega\omega'}^{(b,c)}/\sqrt{\omega'}\right)_{\omega'\rightarrow-\omega'} = \left(\alpha_{\omega\omega'}^{(b,c)}/\sqrt{\omega'}\right)$. Therefore, isolating the $\alpha_{\omega\omega'}^{(b,c)}$ term in (2.16a), the Γ -function can be rewritten using the identity $\Gamma(z+1) = z\Gamma(z)$ to yield

$$\Gamma\left(\delta - \frac{i\omega'}{\kappa_{(b,c)}}\right) = \frac{\Gamma\left(1 - \frac{i\omega'}{\kappa_{(b,c)}}\right)}{-\frac{i}{\kappa_{(b,c)}}(\omega' + i\kappa_{(b,c)}\delta)} \quad , \quad (5.14)$$

where δ has been set equal to zero for the gamma function on the right since its argument is regular at $\omega' = 0$. The leading order effect in (2.16a) can be extracted from the expansion $\Gamma(1 - ax) = 1 + \gamma ax + \mathcal{O}(x^2)$, with γ Euler's constant, to yield

$$\lim_{\omega'\rightarrow 0} \left(\frac{\alpha_{\omega\omega'}^{(b,c)}}{\sqrt{\omega'}}\right) = \frac{i}{2\pi\sqrt{\omega}} \left(\frac{1}{\omega' + i\kappa_{(b,c)}\delta}\right) \left(1 + \gamma\frac{i\omega'}{\kappa_{(b,c)}} + \mathcal{O}(\omega'^2)\right) \quad . \quad (5.15)$$

At late times, the leading order contribution to the Kruskal modes (2.15) in this low ω' -frequency limit is then

$$p_{\omega 00}^{(b,c)}(x)_{\text{low}} \approx \frac{i r_{(b,c)}}{4\pi^2\sqrt{\omega}(r_b^2 + r_c^2)} \int_{-\lambda}^{\lambda} d\omega' \left(\frac{e^{-i\omega't}}{\omega' + i\kappa_{(b,c)}\delta}\right) \quad . \quad (5.16)$$

Since the primary contribution originates from the pole at $\omega' = 0$, one can extend the limits of integration by setting $\lambda = \infty$. For late times $t > 0$, one can use contour integration, with the contour closed in the lower half plane, to obtain

$$p_{\omega 00}^{(b,c)}(x)_{\text{low}} \approx \frac{1}{2\pi\sqrt{\omega}} \left(\frac{r_{(b,c)}}{r_b^2 + r_c^2}\right) \quad . \quad (5.17)$$

Therefore, both sets of Kruskal modes approach constant values at late times. The contribution to $G^{(1)}(x, x')$ that grows linearly in time comes from those Kruskal modes which have already approached constant values. It follows that the $\ell = 0$ contribution to the Hadamard function (2.8) can be approximated at late times by

$$\frac{1}{2}G^{(1)}(x, x') \approx \int_{\omega_0}^{e^{\kappa_b u} \omega_{\text{S.P. min}}^b} d\omega \operatorname{Re} \left\{ p_{\omega 00}^b(x) p_{\omega 00}^{b*}(x') \right\} + \int_{\omega_0}^{e^{\kappa_c v} \omega_{\text{S.P. min}}^c} d\omega \operatorname{Re} \left\{ p_{\omega 00}^c(x) p_{\omega 00}^{c*}(x') \right\} \quad (5.18)$$

$$= \frac{1}{2\pi^2(r_b^2 + r_c^2)^2} (r_b^2 \kappa_b + r_c^2 \kappa_c) t + C_0(r_b, r_c, \omega_0) \quad , \quad (5.19)$$

where C_0 carries no time or space dependence. Note, an arbitrary infrared cutoff ω_0 has been included due to the infrared divergence present at $\omega = 0$. Thus, the Hadamard function growth rate at late times is

$$R_{4D} \equiv \frac{d}{dt} G^{(1)}(t, r, \theta, \phi; t, r', \theta', \phi') = \frac{1}{2\pi^2(r_b^2 + r_c^2)^2} (r_b^2 \kappa_b + r_c^2 \kappa_c) \quad . \quad (5.20)$$

Note that there is no dependence on the infrared cutoff ω_0 . Furthermore, (5.20) is location independent for spatial points between the black hole and cosmological horizons.

In Fig. 7, both analytic expressions for the 2D growth rate (1.1) and the 4D growth rate (5.20) are plotted as a function of the black hole radius r_b . Due to the approximations used in obtaining (5.20), it is useful to compare it with some numerically computed values of the rate. It can be seen that the analytic expression provides a good representation for the actual rate, at least over the range of numerically computed values. Note, it becomes increasingly difficult to numerically compute the 4D Hadamard growth rate for significantly larger values of r_b .

Some interesting features emerge upon comparing the 2D and 4D cases. From (1.1) and (2.11) it can be seen that in 2D SdS the rate diverges as $r_b \rightarrow 0$ since $\kappa_b \sim 1/r_b$ in this limit. This feature does not survive in 4D SdS, where it is the factor of r_b^2 multiplying κ_b in (5.20) that eliminates the divergence as $r_b \rightarrow 0$, and to linear order in r_b (5.20) has the form $R_{4D} = H^3/2\pi^2 + H^4 r_b/4\pi^2 + \mathcal{O}(r_b^2)$. The leading order value is in agreement with that found in [8] for 4D de Sitter space in cosmological coordinates. For intermediate values of

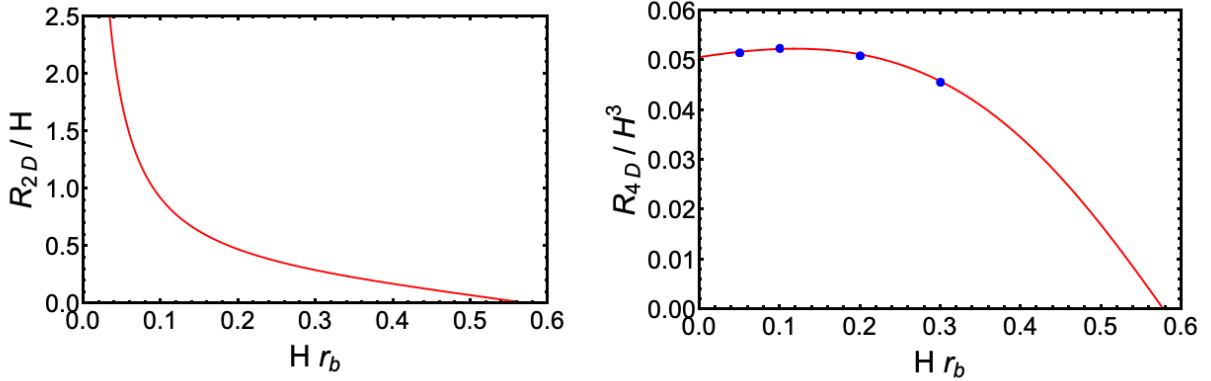


Figure 7. Both the 2D Hadamard growth rate R_{2D}/H (left) and the $\ell = 0$ contribution to the 4D Hadamard growth rate R_{4D}/H^3 (right) are shown as a function of the black hole radius Hr_b . In the 4D case, some numerically obtained values for the growth rate are shown as blue points.

the black hole horizon radius, there exists a maximum which occurs when $Hr_b \approx 0.12$. Both the 2D and 4D Hadamard function growth rates terminate when $Hr_b = Hr_c = \frac{1}{\sqrt{3}}$ due to κ_b and κ_c vanishing in this limit.

VI. DISCUSSION AND CONCLUSIONS

The spherically symmetric contribution to the Hadamard two-point function has been computed in 4D SdS spacetime for a massless minimally-coupled scalar field in the Unruh state. Attention was restricted to points located in the region between the black hole and cosmological horizons. Two sets of modes characterize the Unruh state. One consists of modes that are positive frequency with respect to the Kruskal time on the past black hole horizon and the other consists of modes that are positive frequency with respect to the Kruskal time on the past cosmological horizon.

The mode equation is not separable in either set of Kruskal coordinates, so Bogolubov transformations were used to express the Kruskal modes in terms wave packets of Boulware modes. The Boulware modes were obtained using separation of variables and the equation for the radial part of the modes was solved numerically.

It was found that the Kruskal modes approach nonzero constants at late times for fixed spatial points. Furthermore, the higher the frequency of a mode, the later in time that damping and subsequent approach to a nonzero constant occurs. Similar behavior manifests in 2D where there is no scattering. However, for a given frequency, the nonzero constant value approached in 2D is different than that in 4D.

The contribution to the 4D Hadamard function from the spherically symmetric modes in the Unruh state is found to exhibit unbounded linear growth in terms of the usual static time coordinate for radially separated points in the region between the black hole and cosmological horizons. This same effect was found previously in 2D [7]. However, the rate of growth is suppressed in 4D by scattering effects. In particular, the contribution from the Kruskal modes that are defined on the past black hole horizon is significantly smaller than that from the Kruskal modes that are defined on the past cosmological horizon.

This is corroborated by the derivation of an analytic expression for the rate of growth of the Hadamard function using various approximations. The analytic expression was found to be in good agreement with the numerical results. In the limit that the black hole event horizon vanishes, it agrees with the result found previously for 4D de Sitter spacetime [8] in cosmological coordinates.

There are infrared divergences associated with the Boulware modes which have been seen to have a significant impact not only on the late-time behaviors of the Kruskal modes, but

also on the late-time behavior of the Hadamard function. For 2D Schwarzschild with a delta function potential, it was found [6] there was no linear growth in time of the Hadamard function when scattering effects remove the infrared divergences in the Boulware modes. In 4D SdS, scattering effects do not remove the infrared divergences for the spherically symmetric modes of the massless minimally-coupled scalar field. However, they are expected to remove these divergences for the modes with higher order spherical harmonics. Thus, the only contribution to the Hadamard function that will result in unbounded linear growth is from the spherically symmetric modes.

The linear growth in time of the Hadamard function when the points are split in a radial direction, in coordinates that are natural to the static patch, is a sign of some type of instability. In 2D Schwarzschild spacetime, the linear growth in time of the two-point function leads to a linear growth in time of the quantity $\langle \phi^2 \rangle$ [16]. There is good reason to expect this will also be the case for 4D SdS. However, the stress-energy tensor for the quantum field is not expected to undergo any linear growth in time because it involves two derivatives of the Hadamard function.

The effect found here for SdS is similar in nature to the well-known linear growth in time of the Hadamard function in 4D de Sitter spacetime for the Bunch-Davies state [8]. There it was shown that for de Sitter space there are alternative homogeneous and isotropic vacuum states for which no such instability occurs. Interestingly, the stress-energy tensor for the massless minimally-coupled scalar field in this case has an asymptotic de Sitter-invariant value for these states that is different than the stress-energy tensor for the Bunch-Davies state, which is also de Sitter invariant.

One thing that is different about SdS is the presence of an eternal black hole. The Unruh state is usually thought to be the most physically relevant state for an eternal black hole because it gives a flux of radiation emanating from the black hole equivalent to that predicted by Hawking which occurs at late times for black holes that form from collapse. What is clear from our result is that for a massless minimally-coupled scalar field in 4D SdS, there is some type of instability for the Unruh state. One can ask whether such an instability is likely to persist in models in which the black hole forms from collapse, since then the initial vacuum state for the field is not the Unruh state. This has been tested in 2D in the case of a Schwarzschild black hole that forms from the implosion of a null shell of radiation [7]. In this case, there is no past horizon and there is a well-defined initial vacuum state. For that

state the Hadamard function, at late times and to leading order, has the same linear growth in time as for an eternal Schwarzschild black hole in 2D. Therefore, it is quite possible that the instability found here for the Unruh state in 4D SdS would persist in models in which a black hole in de Sitter space forms from collapse.

ACKNOWLEDGMENTS

We would like to thank Jennie Traschen for a helpful suggestion. P.R.A. would like to thank Northwestern University's Center for Interdisciplinary Exploration and Research in Astrophysics (CIERA) for hosting him during a visit in August of 2023. P.R.A. was supported, in part, by the National Science Foundation under grants No. PHY-1912584 and PHY-2309186 to Wake Forest University. S.P. was supported by the Leverhulme Trust under grant No. RPG2021-299.

-
- [1] S.W. Hawking, *Commun. Math. Phys.* **43** 199 (1975) [Erratum *ibid.* **46** 206 (1976)].
 - [2] G.W. Gibbons and S.W. Hawking, *Phys. Rev. D* **15** 2738 (1977).
 - [3] W.G. Unruh, *Phys. Rev. D* **14** 870 (1976).
 - [4] D. Markovic and W.G. Unruh, *Phys. Rev. D* **43** 332 (1991).
 - [5] S. Tadaki and S. Takagi, *Prog. Theor. Phys.* **83** 941 (1990); *Prog. Theor. Phys.* **83** 1126 (1990).
 - [6] P.R. Anderson, S. Gholizadeh Siahmazgi, and Z.P. Scofield, *Class. Quantum Grav.* **40** 135004 (2023).
 - [7] P.R. Anderson and J. Traschen, *J. High Energy Phys.* **01** 192 (2022).
 - [8] B. Allen and A. Folacci, *Phys. Rev. D* **35** 3771 (1987).
 - [9] P.R. Brady, C.M. Chambers, W. Krivan, and P. Laguna, *Phys. Rev. D* **55**, 7538 (1997).
 - [10] P. Kanti, J. Grain, and A. Barrau, *Phys. Rev. D* **71**, 104002 (2005).
 - [11] P.R. Anderson, A. Fabbri, and R. Balbinot, *Phys. Rev. D* **91** 064061 (2015).
 - [12] L.C.B. Crispino, A. Higuchi, E.S. Oliveira, and J.V. Rocha, *Phys. Rev. D* **87**, 104034 (2013).
 - [13] P. Kanti, T. Pappas, and N. Pappas, *Phys. Rev. D* **90**, 124077 (2014).
 - [14] D. G. Boulware, *Phys. Rev. D* **11**, 1404 (1975).
 - [15] M.R.R. Good, P.R. Anderson, and C.R. Evans, *Phys. Rev. D* **94** 065010 (2016).
 - [16] P. R. Anderson, A. Peak, and S. Gholizadeh Siahmazgi, Unpublished.